

## Supplement - Analytical methods

### 1. Whole Rock XRF and LA-ICP-MS analysis

Whole-rock samples were analysed for major, minor and trace elements. Loss on ignition (LOI) was performed on the rock powders at 850°C for 8 hours to prepare the fused beads for major element analysis. An amount of 1, 2g±0.0005g of the calcined rock powders were mixed with 6g±0.0005g of Lithium Tetraborate (Li<sub>2</sub>B<sub>4</sub>O<sub>7</sub>) and then put in a 1150°C oven for 10-15 minutes to be melted in a Platinum crucible. The crucible was cooled down between each sample, in water from 1150°C to 25°C, cleaned in an ultrasonic bath for 1 minute and put in a 40% citric acid solution heated at 300°C for 10 minutes. The acidic solution is used to take off eventual glass residues inside the crucible.

Pressed pellets for trace element analyses were made by mixing 12g±0.0005g of rock powder with 3g±0.0005g of Hoechst-C wax. This preparation was then put in a steel cylinder and pressed at 9 tons for 30 seconds. The equipment was cleaned between every sample to avoid contamination. Fused beads and pressed pellets were prepared at the Department of Earth Sciences (University of Geneva) in the XRF preparation lab.

The X-Ray Fluorescence (XRF) analyses for both major elements on fused beads and trace elements on pressed pellets were conducted at the Institute of Earth Sciences (University of Lausanne) by Fabio Capponi with an XRF spectrometer PANalytical AxiosmAX. Standards SY-2 and NIM-G were used for calibration. A total of 12 oxide compounds of major elements (SiO<sub>2</sub>, TiO<sub>2</sub>, Al<sub>2</sub>O<sub>3</sub>, Fe<sub>2</sub>O<sub>3</sub>, MnO, MgO, CaO, Na<sub>2</sub>O, K<sub>2</sub>O, P<sub>2</sub>O<sub>5</sub>, Cr<sub>2</sub>O<sub>3</sub>, NiO) and 42 trace elements were measured. Tables 1 and 2 below indicate detection limits and uncertainties of measurements. Analytical conditions are given in tables 1 and 2.

Trace element whole rock composition (, especially Rare Earth Elements-REE), was obtained by Laser Ablation Inductively Coupled Plasma Mass Spectrometry (LA-ICP-MS) analyses which were conducted at the Institute of Earth Sciences, University of Lausanne, with Alexey Ulyanov. The analyses were done on the fused beads previously used for XRF analyses of major elements with CaO from XRF analyses as internal standard and SRM612 as external standard. Analytical conditions are given in Table 3. Whole rock chemistry is reported in tables 1-3 of [doi:10.6084/m9.Figshare.8230787](https://doi.org/10.6084/m9.Figshare.8230787) ~~Electronic appendix B.~~

Table 1. Calibration parameters for whole rock XRF analysis of major elements.

Compound	Calibration range %	Uncertainty 2s absolute mean %	Uncertainty 2s relative mean %
SiO <sub>2</sub>	38-76	0.4	0.7
TiO <sub>2</sub>	0-4	0.01	0.5
Al <sub>2</sub> O <sub>3</sub>	10-30	0.16	0.8
Fe <sub>2</sub> O <sub>3</sub>	1-14	0.07	1
MnO	0-1	0.005	1
MgO	0-16	0.04	0.5
CaO	0-14	0.07	1
Na <sub>2</sub> O	0-9	0.05	1.1
K <sub>2</sub> O	0-15	0.07	1
P <sub>2</sub> O <sub>5</sub>	0-1	0.01	2
Cr <sub>2</sub> O <sub>3</sub>	0-0.1	0.002	4
NiO	0-0.1	0.002	4

Table 2. Calibration parameters for whole rock XRF analysis of minor elements.

Element	Calibration range (ppm)	Absolute error (1s)	Relative uncertainty (2s)	Detection Limit (ppm)	Element	Calibration range (ppm)	Absolute error (1s)	Relative uncertainty (2s)	Detection Limit (ppm)
Sc	0-900	3	6	1	Sn	0-1000	1	2	2
V	0-1000	1	2	2	Sb	0-1000	1	2	3
Cr	0-1000	4	8	1	Te	0-1000	3	6	3
Mn	0-1900	6	16	2	I	0-1000	4	8	3
Co	0-1000	3	6	1	Cs	0-1000	4	8	2
Ni	0-1000	2	4	1	Ba	0-1400	2	4	5
Cu	0-1000	1	2	1	La	0-1000	2	4	7
Zn	0-1000	1	2	1	Ce	0-1000	5	10	5
Ga	0-1000	2	4	1	Nd	0-1000	1	2	3
Ge	0-1000	1	2	1	Sm	0-1000	2	4	3
As	0-1000	2	4	3	Yb	0-1000	3	6	2
Se	0-1000	1	2	1	Hf	0-1000	1	2	2
Br	0-1000	2	4	1	Ta	0-1000	1	2	1
Rb	0-1000	1	2	1	W	0-1000	1	2	1
Sr	0-1400	3	6	1	Hg	0-1000	10	20	4
Y	0-1000	2	4	1	Tl	0-1000	1	2	2
Zr	0-1000	2	4	1	Pb	0-1000	1	2	1
Nb	0-1000	2	4	1	Bi	0-1000	1	2	1
Mo	0-1000	2	4	1	Th	0-1000	2	4	1
Ag	0-1000	2	4	3	U	0-1000	1	2	1
Cd	0-1000	3	6	3					

Table 3. Analytical conditions for LA-ICP-MS

ICP-MS conditions		Laser parameters on-sample	
Repetition rate	20 (Hz)	Repetition rate	10 (Hz)
Laser beam size	75 ( $\mu\text{m}$ )	Laser beam size	105 ( $\mu\text{m}$ )
Energy density	6.0 (J/cm <sup>2</sup> )	Energy density	7.0 (J/cm <sup>2</sup> )
Standard	SRM612		
Internal standard	CaO (XRF values)		
RF power	1430 (W)	Detection limits	
Sample depth	4.0 (mm)	<sup>42</sup> Ca <sup>+</sup>	6.00*10 <sup>6</sup> cps
Extract 1 lens	-2.0 (V)	<sup>139</sup> La <sup>+</sup>	0.71*10 <sup>6</sup> cps
Extract 2 lens	-185.0 (V)	<sup>238</sup> U <sup>+</sup>	1.26*10 <sup>6</sup> cps
Omega bias	-85.0 (V)	<sup>248</sup> Th <sup>+</sup> / <sup>232</sup> Th <sup>+</sup>	0.16%
Omega lens	7.5 (V)	Ca <sup>++</sup> /Ca <sup>+</sup>	0.23%
Cell entrance	-50.0 (V)	<sup>238</sup> U <sup>+</sup> / <sup>232</sup> Th <sup>+</sup>	~113%
Cell exit	-75.0 (V)		
He flow (cell)	1.00 (L/min)		
Ar gas flow on sample	0.83 (L/min)		

## 2. Electron microprobe analysis – EPMA

In situ measurements of major element analysis has been carried out using a JEOL 8200 Electron Microprobe at the University of Geneva, Switzerland. Four sessions (see date analysed in table C.1) were carried out, for which calibration has been realised based on external standards at the beginning of each session. Sulphide minerals were analysed for S, Fe, Cu, Ni, Co, Se, As, Zn, Mo, Si, Ag and Au. Determination limits were stable at 0.01 and 0.02 for Ni/Si and Se, respectively, for the other elements the limits vary depending on the analytical conditions. Operating conditions, peak and background time as well as determination limits for each session is summarized in the table 4, below. Beam size was always set to the minimum possible which reads ‘0’ at the interface of the JEOL software which in reality it may account for a maximum of 2  $\mu\text{m}$  excitation surface and/or volume (see arrow on 2<sup>nd</sup> example of method A in Tab.4.). The EPMA values reported in this study (Tab.1, and Fig.7 and 8) correspond to a single point of a single mineral phase composing the sulfide inclusion. Only sulfide phases that were big enough ( $>2 \mu\text{m}$ ) were analysed, making sure the beam was carefully placed on a single mineral phase. For the cases where a mineral phase composing a sulfide inclusion was smaller than  $2 \mu\text{m}$  the SEM has been used instead in order to have a qualitative value. When the analysis program was run through the night a beam alignment check was required, in case of any offset.

From 680 sulfide measurements obtained, 503 were above a total (%) of 94, 232 $>$ 98 and 36 $>$ 99.5. Only measurements that resulted in totals higher than 94% have been considered. From those 503, Cu and Ni were above detection/determination limit for 489 and 496 values, respectively. Out of 503 Ag and 196 Au sulfide measurements obtained, only 82 and 31 values, respectively, resulted in concentrations above detection/determination limit.

Low totals for the remaining 177 of sulfides analysed, can be caused by; 1) interference resulting from the excitation of the surrounding host mineral, particularly when the sulfide inclusion is too small ( $<4 \mu\text{m}$ ), for this reason the Si signal can be used as an indicator, 2) “bad” surface flatness, especially for the cases where the hardness of the host mineral differs significantly relative to the one of the sulfide inclusion and 3) oxygen concentrations that cannot be directly measured with EPMA/SEM.

Electron microprobe data are reported in table [4 in doi:10.6084/m9.Figshare.8230787C.3](https://doi.org/10.6084/m9.Figshare.8230787C.3) (Electronic appendix C).

Table 4. Calibration analytical conditions for EPMA sulfide analysis.

Session-Date	1 <sup>st</sup> –May.25.17	2 <sup>nd</sup> . Nov.24.17	3 <sup>rd</sup> – Jan.8.18	4 <sup>th</sup> – Nov.5.18
voltage-Kv/current nA	15/20	20/20	20/20	20/20
Element analysed — stnd used	Time of analysis on peak-s/background-s/determination limit (only for minor elements)-median			
S-FeS/Pyrite	20/10	20/10	20/10	20/10
Fe-FeS/Pyrite	20/10	20/10	20/10	20/10
Cu-Cu pure	20/10/0.03	20/15/0.01	20/15/0.01	20/15/0.01
Ni-Ni pure	40/20/0.01	30/15/0.01	30/15/0.01	60/30/0.01
Co-Co pure	30/15/0.01	NA	NA	NA
Se-CdSe	30/15/0.02	20/10/0.02	20/10/0.02	30/10/0.02
As-GaAs	30/15/0.02	30/15/0.02	30/15/0.03	30/15/0.02
Zn-ZnS	40/20/0.03	20/10/0.02	20/10/0.02	NA
Mo-Mo pure	NA	NA	NA	20/15/0.01
Si-Olivine	NA	20/10/0.01	20/10/0.01	20/10/0.01
Ag-Ag pure	40/20/0.03	40/20/0.01	40/20/0.01	40/20/0.01
Au-Au pure	NA	40/20/0.03	NA	40/20/0.1

### 3. ImageJ software and Bulk area reconstruction of sulfide composition

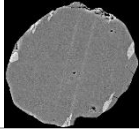
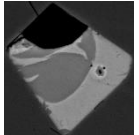
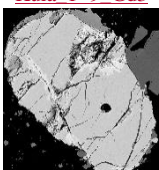
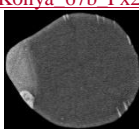
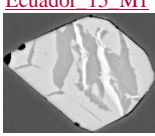
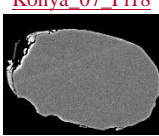

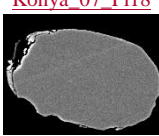

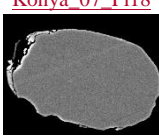

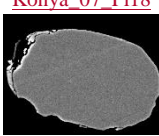
An image analysis software (ImageJ©1.38) was used in order to obtain the relative proportions of the various mineral phases composing a sulfide inclusion by analysis reflected and BSE microphotographs. The comparison of these mineral phase proportions (and therefore the mss and iss relative area %) of the most primary sulfides for each study area, can give an indirect information on the initial metal amounts of the magmas characterising the different study areas investigated. In total 163 sulfides were processed with ImageJ of which 126 (Kula=25, Itecektepe=16, Elmadag=10, Beydagi=15, Konya=25, Ecuador=35) have been classified as Type-2 sulfides, which is the only sulfide type present in all study areas. The results are depicted at the box-plot of Fig.9.

This method has been also applied by other researchers; Nadeau et al., 2010 (investigating the Merapi volcano) on 5 sulfides resulting in mss and iss proportions of  $81 \pm 7$  and  $19 \pm 7$ , respectively and by Chang et al., 2018 while investigating Type-2 sulfides (in arc magmas of Santa Rita and Cherillos/New Mexico) by LA-ICP-MS, indicating that the more Cu-rich/iss mineral phases take less/equal to 20 vol% relative to the Cu-poor/mss.

In addition to the process mentioned above and in order to have an general idea on the reconstructed bulk area ~~The reconstruction of the bulk~~ sulfide composition, ~~the was based on~~ area (%) of mineral modal abundances calculated by ~~an image analysis software (ImageJ©1.38) were weighed with and the values obtained by~~ EPMA analysis, for all investigated areas (including Ecuador). Only analysis resulting in totals above 94 % have been included in the reconstruction. Not all sulfides that were processed by an image analysis software had corresponding EPMA values for all mineral phases composing the sulfide inclusions. Because of that three main methods have been applied for the bulk area reconstruction (see Tab. 5);. The results of both ImageJ and bulk reconstruction are shown in Table 5 in doi:10.6084/m9.Figshare.8230787.

This method of combining modal abundances resulting from image analysis and EPMA compositions has been applied before by Greau et al., 2013 working on sulfides in eclogites (Roberts Victor/South Africa) and by Shaw, 1997 working on sulfides in mantle xenoliths (West Eifel volcanics/Germany). for those cases in table C.2. only the area has been reported (e.g. Elmadag, Itecektepe study areas). For the cases where a mineral was too small ( $<2\mu\text{m}$  in size) for EPMA analysis, the SEM value has been used instead. Therefore in table C.2. under the column entitled "methods" is indicated "only area", "EPMA" or "SEM". For the cases where neither EPMA, nor SEM had been obtained for one of the mineral phases composing the sulfide inclusion, a median EPMA value of the same mineral phase, analysed in the same thin section has been attributed instead and has been indicated in table C.2. as "extra". Only the area and not the volume have been calculated in this study. However in order for the reader that wants to have an initial estimate of the volume, the size and shape have been reported for every sulfide inclusion as well.

Table 5. Representative sulfide examples have been reported for each bulk area reconstruction method. Every method corresponds to a different case; A) Cases where reliable EPMA values (value corresponding to only one phase/not mixed signals and with totals above 94%) had been obtained from all mineral phases composing the sulfide inclusion, B) Cases where only one/some of the phases had corresponding reliable EPMA values and where an SEM value was used for the remaining phase instead. The SEM value has been shown in the table with a star (\*). This remaining phase it was either too small ( $<2\mu\text{m}$ ) or it revealed an EPMA total below 94%. C) Cases where only one/some of the phases had corresponding reliable EPMA values and the remaining phase did not have a corresponding EPMA (total $>94\%$ ) nor an SEM value. For those cases a median a median EPMA value (indicated by a ^-symbol) of the same mineral phase, analysed in the same thin section has been attributed instead. The name of each sulfide/sample has been inserted over every figure, sulfides of these figures are generally around 20  $\mu\text{m}$  and always  $<100$  and  $>10$   $\mu\text{m}$  please see Tab.5 in doi:10.6084/m9.Figshare.8230787 for exact size in  $\mu\text{m}$ .

		Sulfide		Jimage (area %)		EPMA or SEM* (wt %)			
				mss	iss	S	Cu	Fe	Ni
Method A applied on 47 sulfides	Type-1	Kula_18_OI1 	Po Pn	94 6		38.7*94 37.9*6	0.04*94 0.05*6	57.1*94 55.14*6	3.1*94 5.2*6
	Type-4	Reconstructed Konya_37_Mt2 	Cp Bn		55 45	32.6*55 26.60*45	39.2*55 57.62*45	27.6*55 16.33*45	0.01*55 0
	Type-2	Reconstructed Kula_1_9_Gd3 	Po Cp	88	12	38.57*88 34.75*12	0.45*88 24.57*12	60.68*88 38.81*12	0.1*88 0.05*12
	Type-2	Reconstructed Konya_67b_Px2 	Po Pn* Cp	89 2	11	39.4*89 26.3*2 36.8*11	0.04*89 0 27.8*11	55.2*89 34.6*2 33.4*11	3.2*89 38.4*2 0.5*11
	Type-4	Reconstructed Ecuador_15_M1 	Cp* Bn Dp*		39 56 5	20.7*39 16.3*56 16*5	50.6*39 67.1*56 73.6*5	28.7*39 16.5*56 10.5*5	
	Type-2	Reconstructed Konya_07_P118 	Po Cp^	97	3	39.6*97 35.15*3	0.06*97 25.7*3	58.7*97 37.2*3	0.14*97 0.04*3
Method B applied on 9 sulfides	Type-4	Reconstructed Kula_01_OI2 	Po Cb^	97	3	37.9*97 35*3	0.3*97 24.5*3	56*97 38.3*3	4.3*97 0.4*3
	Type-2	Reconstructed Konya_07_P118 	Po Cp^	97	3	39.6*97 35.15*3	0.06*97 25.7*3	58.7*97 37.2*3	0.14*97 0.04*3
	Type-1	Reconstructed Kula_01_OI2 	Po Cb^	97	3	37.9*97 35*3	0.3*97 24.5*3	56*97 38.3*3	4.3*97 0.4*3
Method C applied on 44 sulfides	Type-2	Reconstructed Konya_07_P118 	Po Cp^	97	3	39.6*97 35.15*3	0.06*97 25.7*3	58.7*97 37.2*3	0.14*97 0.04*3
	Type-1	Reconstructed Kula_01_OI2 	Po Cb^	97	3	37.9*97 35*3	0.3*97 24.5*3	56*97 38.3*3	4.3*97 0.4*3
	Type-2	Reconstructed Konya_07_P118 	Po Cp^	97	3	39.6*97 35.15*3	0.06*97 25.7*3	58.7*97 37.2*3	0.14*97 0.04*3

#### 4. Distinguishing criteria between hydrothermal and magmatic sulfide inclusions under the microscope.

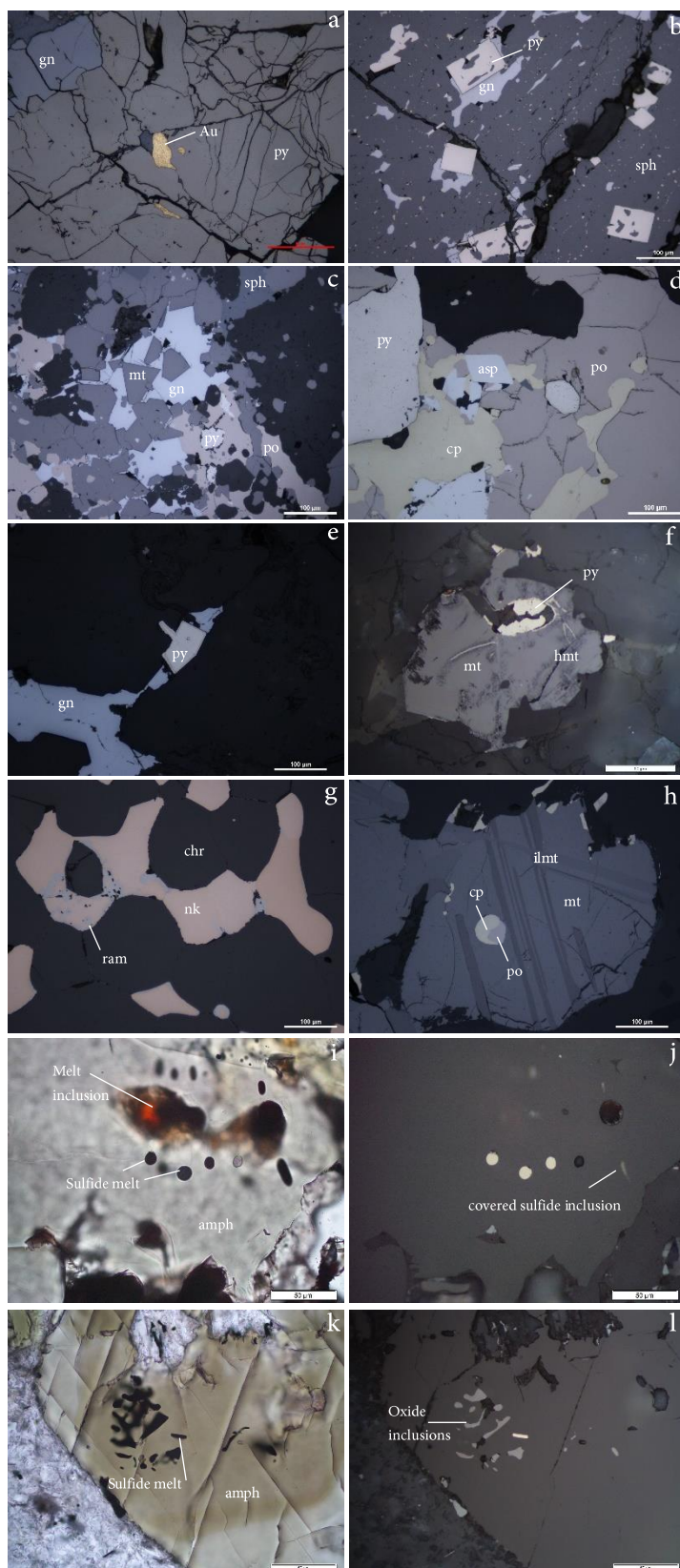
Although, both hydrothermal and magmatic sulfides are composed of sulfur (anion) and of one or more metal (cation/s), they are a result of different formation processes. Hydrothermal sulfide minerals are a product of metal precipitation by an aqueous fluid phase whereas magmatic sulfide minerals are formed by sulfide liquid exsolution from a melt. According to the geological context that characterises the investigated rock sample, both sulfide categories can be found either in the groundmass/matrix or as inclusions inside other mineral phases. However depending on the occurrence, shape, texture and sulfide composition, a number of characteristic features can be used to distinguish hydrothermal from

magmatic sulfide minerals. In general in fresh/not altered and barren/not mineralised volcanic rocks (like the rocks investigated in this study) small sulfide inclusions hosted by silicate and oxide minerals that do not show any surrounding fracturing and no oxide replacement are likely to be magmatic. A detailed petrographic study applying the criteria mentioned below combined with SEM and Raman spectroscopy will confirm the origin of the studied sulfide inclusion phase.

- i) Occurrence: Hydrothermal sulfide inclusions can be observed as filling material inside mineral fractures or as secondary phases which replaced a primary magmatic sulfide hosted by silicate and oxide minerals. In addition hydrothermal sulfides may be found in a fluid inclusion whereas magmatic sulfides in a melt inclusion.
- ii) Shape: Hydrothermal sulfide inclusions have mostly irregular idiomorphic to sub-idiomorphic shapes whereas magmatic sulfide inclusions are characterised by rounded/ellipsoidal ‘droplet-like’ or even angular/rectangular pseudo-idiomorphic shapes (when the sulfide phase has solidified according the structural planes of the host mineral and not according to the sulfide minerals growing structure).
- iii) Texture: Hydrothermal sulfides are often characterised by; crystal zoning (sometimes optical as well as chemical), spongy/vesicular appearance and are often associated with cracks, veining and alteration whereas magmatic sulfides look fresh with no visible crystal zonation. The latter when enclosed (no signs of fracturing) in the host mineral, they do not show alteration.
- iv) Composition: There are some mineral phases that by definition cannot be magmatic because they are a product of lower temperature formation like sphalerite, galena, enargite, etc.
- v) Size and abundance: Although it will not always be the case, in general magmatic sulfide inclusions that are present in felsic rocks have smaller sizes (<100µm) and are less abundant (<0.1 area %, e.g. Savelyev et al., 2018) than hydrothermal sulfides.
- vi) Accessory minerals: The study of associated to the sulfide, accessory minerals can provide useful information. For example, if a sulfide co-exists with silicate melt/glass in the same host mineral then this sulfide is most likely of magmatic origin.

Nevertheless, distinguishing hydrothermal from magmatic sulfide inclusions can be difficult when a sample carrying magmatic sulfides has been replaced and overprinted by hydrothermal sulfide minerals. In these cases it is possible to find, for example, magmatic chalcopyrite co-existing with hydrothermal chalcopyrite. Although the shape, texture and occurrence may help to differentiate those two types of chalcopyrite when a mineral hosting a magmatic sulfide inclusion fractures, those cracks can be used by the hydrothermal fluid to enter the structure of the host mineral and alter/dissolve the magmatic sulfide inclusion by oxide replacement.





**Figure 1.** Microphotographs showing characterising features of hydrothermal (a-e) and magmatic (f-l) sulfides. Note the mineral properties when it occurs as inclusion inside other mineral phases; a) Irregular-shaped native gold inclusions inside pyrite, note the extensive fracturing, some of the cracks have been filled with sphalerite, (Pataz deposit/Peru, observed by 50x-oil lense), b) Idiomorphic pyrite crystals partly replaced by sphalerite, sphalerite matrix carrying chalcopyrite micro-inclusions and galena filling textures (Pataz deposit/Peru), c) Idiomorphic magnetite in galena, sub-idiomorphic partly altered in the rims pyrite inside pyrrhotite and sub-idiomorphic to rounded pyrrhotite inside magnetite (Faro deposit), d) Idiomorphic arsenopyrite and sub-idiomorphic pyrite hosted by pyrrhotite-chalcopyrite matrix, note the cracks in pyrrhotite in which a reaction/intermediate product occurs (Dale Head deposit/Britain), e) Idiomorphic bravoite (chemically zoned Co-Ni bearing pyrite) occurring together with galena interstitially filling the spaces between gangue minerals (Maubach deposit/Germany), f) Fractured, altered and replaced magmatic sulfide, now showing pyrite composition, in magnetite with hematite occurring in the cracks (Beydagi volcanics/Turkey), g) Nickeline partly replaced by rammelsbergite occurring interstitially between cumulate chromite crystals (Los Jarales/Ronda Peridotite/Spain), h) Round sulfide inclusion of chalcopyrite and pyrrhotite inside magnetite that shows ilmenite and ulvospinel exsolution lamellae (Routivare/Sweden), i-j) Magmatic sulfide inclusion trail occurring with melt inclusions in plagioclase host, sulfides are round and mostly composed of pyrrhotite (Kula volcanics-LP16018/Turkey), k-l) Magmatic elliptical-shaped sulfide composed of mostly pyrrhotite occurring together with oxide inclusions in amphibole host (Konya volcanics-bd16065/Turkey). For more examples of magmatic sulfides (hosted also in other silicate minerals, in oxide phases and melt inclusions see Figs.4-6). All figures correspond to reflected light (parallel Nicolls) microscope photos except figures i and k which correspond to transmitted light (parallel Nicolls). Samples (a-h) were provided by Dr. Kalin Kouzmanov from the University of Geneva, Switzerland.

## 5. Limitations of the method and approach

We are aware that, despite the efforts made in this study to investigate a large number of thin sections, the population considered remains likely under sampled and therefore the results of this 'pilot' study cannot generalise for all volcanic centers characterised by the same geodynamic setting. However, the aim of this work is to evaluate first order (large) variations in the textural and compositional characteristics of magmatic sulfides collected from different geodynamic contexts and it is likely that the investigated population is able to provide this.

Additionally, the sulfide bulk composition area reconstruction in multiphase sulfide inclusions can be subject to limitations, like the uncertainty in translating the 2-dimensional surface reconstruction to the real 3-dimensional distribution of the different mineral phases within the solid inclusion or the representativeness of the single spot composition measured by EMPA on one mineral phase with respect to the entire area of the mineral phase. We tried to obviate these problems by investigating and quantifying a large number of sulfide inclusions in several sections (which should reduce the cut effects on 2-dimensional distribution of the mineral phases) and by coupling a representative analytical spot with BSE images providing a means to evaluate the compositional homogeneity of the mineral phase investigated and the representativeness of the spot analysis. We highlight that this approach was taken in order to evaluate the entire population of sulfide inclusions occurring in magmatic rocks, a great part of which are hosted by magnetite. The latter inclusions cannot be measured by bulk LA-ICPMS methods due to the opacity of the magnetite host.